Neurophotonics

Neurophotonics.SPIEDigitalLibrary.org

Inhibitory effect of 980-nm laser on neural activity of the rat's cochlear nucleus

Bin Jiang
Wensheng Hou
Nan Xia
Fei Peng
Xing Wang
Chunye Chen
Yi Zhou
Xiaolin Zheng
Xiaoying Wu

SPIE.

Bin Jiang, Wensheng Hou, Nan Xia, Fei Peng, Xing Wang, Chunye Chen, Yi Zhou, Xiaolin Zheng, Xiaoying Wu, "Inhibitory effect of 980-nm laser on neural activity of the rat's cochlear nucleus," *Neurophoton.* **6**(3), 035009 (2019), doi: 10.1117/1.NPh.6.3.035009.

Inhibitory effect of 980-nm laser on neural activity of the rat's cochlear nucleus

Bin Jiang,[a] Wensheng Hou,[a,b,c] Nan Xia,[a,d,*] Fei Peng,[a] Xing Wang,[a,b] Chunye Chen,[a,b] Yi Zhou,[e] Xiaolin Zheng,[a,b,c] and Xiaoying Wu[a,b,c,*]

[a]Chongqing University, Ministry of Education, Key Laboratory of Biorheological Science and Technology, Chongqing, China
[b]Chongqing University, Chongqing Collaborative Innovation Center for Brain Science, China
[c]Chongqing University, Chongqing Key Laboratory of Artificial Intelligence and Service Robot Control Technology, Chongqing, China
[d]Qingdao University, Shandong Provincial Key Laboratory of Digital Medicine and Computer-assisted Surgery, Qingdao, Shandong, China
[e]Chinese Army Medical University, Department of Neurobiology, Chongqing Key Laboratory of Neurobiology, Chongqing, China

Abstract. Near-infrared radiation (NIR) has been described as one of the highest-resolution tools for neuromodulation. However, the poor tissue penetration depth of NIR has limited its further application on some of the deeper layer neurons *in vivo*. A 980-nm short-wavelength NIR (SW-NIR) with high penetration depth was employed, and its inhibitory effect on neurons was investigated *in vivo*. In experiments, SW-NIR was implemented on the rat's cochlear nucleus (CN), the auditory pathway was activated by pure-tones through the rat's external auditory canal, and the neural responses were recorded in the inferior colliculus by a multichannel electrode array. Neural firing rate (FR) and the first spike latency (FSL) were analyzed to evaluate the optically induced neural inhibition. Meanwhile, a two-layered finite element, consisting of a fluid layer and a gray matter layer, was established to model the optically induced temperature changes in CN; different stimulation paradigms were used to compare the inhibitory efficiency of SW-NIR. Results showed that SW-NIR could reversibly inhibit acoustically induced CN neural activities: with the increase of laser radiant exposures energy, neural FR decreased significantly and FSL lengthened steadily. Significant inhibition occurred when the optical pulse stimulated prior to the acoustic stimulus. Results indicated that the inhibition relies on the establishment time of the temperature field. Moreover, our preliminary results suggest that short-wavelength infrared could regulate the activities of neurons beyond the neural tissues laser irradiated through neural networks and conduction *in vivo*. These findings may provide a method for accurate neuromodulation *in vivo*. [DOI: 10.1117/1.NPh.6.3.035009]

Keywords: short-wavelength near-infrared radiation; cochlear nucleus; neuromodulation; neural inhibition.

Paper 19005RR received Jan. 22, 2019; accepted for publication Jul. 18, 2019; published online Aug. 27, 2019.

1 Introduction

Neuromodulation is an efficient technique to study how neural activities operate brain functions, and it requires not only effective neural stimulation but also high precision.[1–4] Among all neuromodulation techniques, pulsed near-infrared (NIR) radiation (wavelength between 1850 and 2120 nm) is considered a strong candidate for precise control of neural activity, due to its high stimulating spatial resolution and contact-free advantages.[5–10] NIR has been widely used to modulate the functionality of the peripheral[5–7,11,12] and the central nervous system.[8–10,13,14] Most previous studies have focused on NIR-induced neural activation;[6–9,15] neural suppression is also indispensable in neuroscience, especially for brain disorder treatment.[16–18]

Recently, evidence has gradually appeared showing that NIR could reversibly inhibit unwanted neural activity[16,19,20] or block neural signal propagation with high precision.[21,22] However, current NIR-based neural inhibition experiments have mostly been carried out on peripheral nerves,[21,23] neurons cultured *in vitro*,[19,20,24] and superficial cortex;[10] research investigating the inhibitory effect of NIR on neurons in deeper layers *in vivo* has been limited. The main reason for this, in addition to the complexity of the central nervous system and complex neural responses to NIR,[8,10] has been the poor tissue penetration depth of NIR. The maximum penetration depth of NIR used in previous works was about 1100 μm,[25] but target neurons *in vivo* such as hippocampal neurons are located much deeper,[2] so it has been a challenge for the conventional NIRs to modulate such deeper neurons *in vivo*.

Compared with NIR, short-wavelength NIR (SW-NIR, wavelength from 800 to 1100 nm) has a much higher penetration depth in tissues (at least 2.5 cm),[26] which is very beneficial for neuromodulation by laser *in vivo*. Recently, SW-NIR with wavelengths of 808 and 980 nm has been successfully applied to activate the auditory nerve and neurons in the primary motor cortex.[27–31] Different from the mechanism of optically induced neural activation, neural inhibition of NIR relies on the optically induced tissue baseline temperature increasing,[16,19,20,32] and evidence shows that neural activities can be effectively inhibited when tissue temperature is increased by 3°C to 8°C.[16,32] Besides its strong penetrating ability, SW-NIR also has a low tissue absorption coefficient, which may affect the thermal interaction between laser and target tissue. Therefore, it is unknown whether SW-NIR could effectively elevate the tissue temperature to reach the temperature threshold for neural inhibition. Fortunately, the inhibition effect of 980-nm laser pulse on neurons was recorded in our preliminary experiment,[33] but whether this inhibitory effect of SW-NIR on neurons is associated with the tissue baseline temperature increase and how SW-NIR

*Address all correspondence to Nan Xia, E-mail: loojourney@163.com; Xiaoying Wu, E-mail: wuxiaoying69@163.com

regulates neurons *in vivo* are as yet unexplored. Furthermore, most of the existing studies have directly recorded the responses of neurons irradiated by lasers; few studies have been done to evaluate the infrared neuromodulation of neural networks and conduction *in vivo*.

To better understand the effect of SW-NIR on neurons *in vivo*, a 980-nm fiber-coupled laser was used to modulate CN neural activities of the Sprague–Dawley rat (SD rat). Optical stimulation parameters and different stimulation paradigms were investigated. Laser fiber was placed on top of the rat's CN, the auditory pathway was activated by pure-tones given from the external auditory canal, and neural responses were recorded from inferior colliculus (IC). Neural firing rate (FR) and the first spike latency (FSL) were analyzed to evaluate the optically induced neural inhibition. Results showed that 980-nm laser pulse could reversibly and repeatedly inhibit acoustically induced neural activities in CN: with the increase of laser pulse energy, the neural inhibition rate increased steadily and reached up to 70% when the laser radiant exposure was 39.06 J/cm^2 (pulse power: 6 W, pulse width: 5 ms). Experiments under different stimulation paradigms indicated that the inhibition relies on the establishment time of the temperature field in tissue induced by laser pulse.

2 Materials and Methods

Twelve healthy adult female SD rats (weight 200–300 g, age 6–8 weeks, not in the estrous cycle) were used in this study because of their better hearing sensitivity than male SD rats.[34] All rats were purchased from the Experimental Animal Center of the Daping Hospital. The procedures were performed in accordance with protocols of the Care and Use of Laboratory Animals approved by the Army Medical University.

2.1 *Modeling of Laser-Induced Temperature Changes*

A two-layered finite-element method of CN was established in COMSOL Multiphysics (version 5.3, Stockholm, Sweden), including a cerebrospinal fluid (CSF) layer (thickness: 0.1 mm) and a gray matter (GM) layer (thickness: 1 mm). Laser pulse power varied from 0.1 to 9 W (pulse width: 5 ms), and pulse width varied from 0.1 to 30 ms (pulse power: 6 W). Laser fiber diameter and numerical aperture were set to 200 μm and 0.22, respectively. The distance of optical fiber tip to the CN was 250 μm and the irradiation radius of the laser fiber was calculated by Eq. (1). (A schematic diagram is shown in Fig. S1 in the Supplementary Material.) The thermal parameters used for simulation are summarized in Table 1.

$$R = \sqrt{\frac{\sin^2 \alpha Z^2}{1-\sin^2 \alpha}} + R_a, \tag{1}$$

where α is the spreading angle ($\sin \alpha = 0.22$), R_a is the fiber core radius (100 μm), and Z is the distance from fiber to tissue (250 μm).

Laser-induced temporal and spatial temperature changes in CN were calculated using the Pennes bioheat equation, as follows:[38]

$$\rho C \frac{\partial T}{\partial t} + \nabla \cdot (-k \nabla T) = \rho_b C_b \omega_b (T_b - T) + Q_{met} + Q_{laser}, \tag{2}$$

Table 1 Thermal parameters of the CN tissue.

Thermal parameter	Value	Units	Reference
C_GM	3850	J/(kg.K)	35
C_CSF	3850	J/(kg.K)	35
C_blood	3850	J/(kg.K)	35
T_GM	310.35	K	35
T_CSF	310.25	K	35
T_blood	309.35	K	35
r_GM	1080	kg/m^3	35
r_CSF	1000	kg/m^3	35
r_blood	1060	kg/m^3	35
Q_{met}	15575	W/m^3	36
ω_b	0.17467	1/s	36
K_GM	0.52	W/(m.K)	36
K_CSF	0.58	W/(m.K)	37

where ρ is the tissue density, C is the tissue-specific heat, k is the tissue thermal conductivity, T is the tissue temperature, ρ_b is the blood density, ω_b is the blood perfusion, C_b is the blood specific heat capacity, T_b is the blood temperature, t is the calculating time, Q_{met} is the metabolic heat generation, and Q_{laser} is the optical heat source.

The optical heat source Q_{laser} was calculated by Eq. (3).[39] The scattering (μ_s), absorption (μ_a) coefficients of GM and CSF for 980-nm laser and 1850-nm laser were obtained from the literature[40–42] (see Table 2). Anisotropy (g) was assumed to be equal to 0.9:

$$S(r,z) = \mu_\alpha (1-R)\varphi_0 \exp\left[-0.5\frac{r^2}{{\omega_0}^2}\exp(-\mu_{sz}) - \mu_{tz}\right] \times \exp\left[-4\frac{(t-\tau)^2}{\tau^2}\right], \tag{3}$$

Table 2 Optical parameters used in the heating model.

Optical parameter	Value	Units	Reference
$\mu_{\alpha 980\text{-nm}}$_CSF	48	1/m	41
$\mu_{\alpha 980\text{-nm}}$_GM	60	1/m	41
$\mu_{s980\text{-nm}}$_GM	5500	1/m	40, 41
$\mu_{s980\text{-nm}}$_CSF	10	1/m	40, 41
$\mu_{\alpha 1850\text{-nm}}$_CSF	960	1/m	42
$\mu_{\alpha 1850\text{-nm}}$_GM	960	1/m	42
$\mu_{s1850\text{-nm}}$_GM	1000	1/m	42
$\mu_{s1850\text{-nm}}$_CSF	0	1/m	42

where μ_α is the absorption coefficient, μ_s is the scattering coefficient, $\mu_t = \mu_s + \mu_\alpha$ is the tissue attenuation coefficient, and φ_0 is the incident light flux density.

2.2 *Animal Surgery and Preparation*

Surgical and neural data collection methods have been previously described.[33] Animals were anesthetized by an intraperitoneal injection of urethane (1.2 g/kg body weight in sterile saline). Depth of anesthesia was assessed by toe pinch every 30 to 60 min, maintaining with 0.16 g urethane/kg body weight to ensure the anesthesia state of animals. The animal was moved to the sound-attenuating room, where the ambient noise floor was 25-dB sound pressure level (SPL). The hairs on the auricle, head, and neck of the animal were removed. Tracheotomy was performed on the animal to assist animal respiration. The animal's head was secured on a stereotaxic instrument (ST-SND-B, Chengdu Instrument Factory, Chengdu, China) with ear bars through both sides of the external auditory canal. Skin and membranous tissue were removed to expose the skull. Three holes were made adjacent to the bregma, about 3 mm apart, using a motorized dental drill (STRONG90+102L, South Korea) with a drill bit size of 1-mm diameter. Three 1.4-mm stainless steel self-tapping screws (1.4×3.6 mm^2) were fastened on the skull through the holes. The tip of a custom-made head holder was placed on the top of the screws and fixed by dental acrylic. After dental acrylic solidified, the ear bars were removed to free the animal ears. The skull and occipital bone above the cerebellum were ground off using a dental drill to expose the edge of the cerebrum and the cerebellum. Left cerebellar hemisphere was sucked away by a homemade syringe straw to expose the left cochlear nucleus (CN). Then, the right cerebrum was partially removed to expose the right IC (see Fig. 1). The entire experiment was carried out on a heating pad connected with the thermostatic bath (HSS-1B, Chengdu Instrument Factory, China), and the animal's body temperature remained constantly at 38°C.

2.3 *Acoustic Stimulation*

Sound stimulation was given by the earphone (Beyerdynamic DT 770, Germany) placed in the sound-attenuating room. The earphone was placed at a distance of 1 cm from the ipsilateral ear canal with the exposed CN. The acoustic stimulation signals were generated by LabVIEW (LabVIEW2012, National Instruments, Austin, U.S.A). Acoustic clicks (square waveforms with 100-μs pulse width, 9-Hz repetition rate) and pure tone bursts (12-ms duration, 1-ms rise/fall) were used to detect the animal hearing threshold before and after surgery. The frequency for the pure tone bursts started from 0.5 kHz and was increased in eight steps per octave over seven octaves to 32 kHz. The repetition rate of pure tone bursts was 4 Hz. Sound levels at each frequency began at 80 dB SPL and were attenuated in steps of 5 to 30 dB SPL. A 50-ms white noise was used to search neurons in IC, and pure tone from 0.5 to 32 kHz was used to determine the neural characteristic frequency (CF) for each neuron recorded by the electrode.

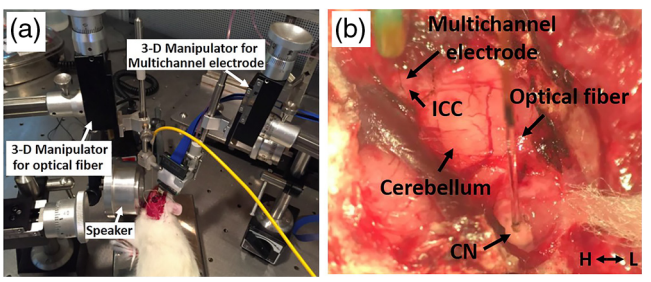

Fig. 1 Experimental set-up. (a) The placement of speaker, the optical fiber and the recording electrode. (b) Surgical exposure for laser stimulation and signal recording. Optical fiber was placed on the surface of the CN and a multichannel recording electrode was implanted in IC.

2.4 *Acoustical and Optical Co-Stimulation Protocol*

The optical stimulation was generated by a 980-nm laser (Associated Opto-Electronics Corp., Chongqing, China) coupled with a 200-μm fiber, and the fiber was held by a three-dimensional (3-D) micromanipulator (WST-3, Chengdu Instrument Factory, Sichuan, China). The distal tip of the optical fiber was placed on the CN surface. The laser parameters included laser pulse width and laser pulse power: laser pulse width ranged from 1 to 5 ms (in 2-ms step, pulse power: 6 W), and laser pulse power ranged from 1 to 6 W (in 1-W step, pulse width: 5 ms). The corresponding radiant exposures were ranging from 6.51 to 39.06 J/cm^2 at a 5-ms pulse width. The stimulation frequency was 4 Hz. The output power from the optical fiber was measured before experiment using a laser power meter (PowerMax-Pro, Santa Clara, U.S.A).

The acoustic stimulus was pure-tone. The frequency of pure-tone was matched to a certain frequency, which was consistent with CF of IC neurons. The sound level of pure-tone was fixed at 80 dB SPL, and the repetition rate was fixed 4 Hz.

Stimulation paradigms of acoustic and optical stimulus included four types: laser pulse was delivered 5 ms prior to acoustic stimulus; acoustic stimulus and laser pulse were given simultaneously; laser pulse and acoustic stimulus end at the same time; and laser pulse was given immediately right after the acoustic stimulus [see Fig. 9(a), row 1].

2.5 *Auditory Brainstem Response Measurement*

Three stainless steel needles (25-mm length and 0.35-mm diameter, Suzhou Hua Tuo Medical Instruments Co., Ltd., Suzhou, China) were used to record auditory brainstem response (ABR). The stainless steel needle electrodes were insulated with polydimethylsiloxane, which expects that the two ends of the electrodes were exposed. The record electrode was placed on the top of the skull. The reference electrode was placed at the left mastoid and the ground electrode was placed on the tip of the nose. The electrodes were connected to the Cerebus physiological signal acquisition system (Cerebus 6.01, Blackrock Microsystems, Salt Lake City, U.S.A). The sampling rate was set to 30 kHz. The recorded signal was bandpass filtered between 300 and 3000 Hz. ABRs were averaged at least 1350 times.

2.6 *Neural Response Recording*

Neural responses were recorded by a 16-channel penetrating electrode array (A1x16-5 mm-150-177, Neuronexus, Ann Arbor, Michigan) placed in IC. The electrode was fixed in front of a hydraulic micromanipulator (50-12-1C Hydraulic Probe Drive and 50-12-9 Manual Drum Unit, FHC, Chicago, U.S.A) and was inserted into the IC on a dorsolateral to ventromedial trajectory at about 30 deg off the parasagittal plane with the

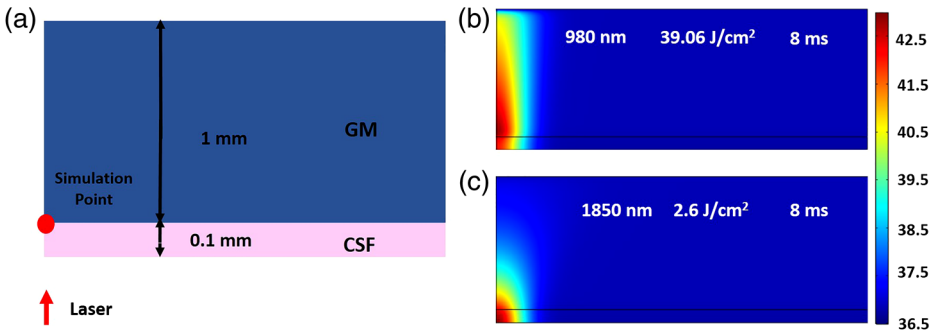

Fig. 2 Temperature spatial distributions. (a) Simulation diagram. Red dot and red arrow in (a) represent the temperature recording point and the laser, respectively. Tissue temperature spatial distributions simulation of (b) 980-nm laser (pulse power: 6 W, pulse width: 5 ms) and (c) 1850 nm laser (pulse power: 0.4 W, pulse width: 5 ms).

accuracy of 1 μm. The ground electrode was placed on the temporal bone under the skin.

Multiunit and single-unit responses (spikes) from each channel were recorded by Cerebus multichannel physiological signal acquisition system. For spike recording, a bandpass filter with the range of 300 to 3000 Hz was used and the sampling rate was set at 30 kHz. The synchronization signals from the optical and acoustical stimuli were also collected for offline data analysis.

2.7 *Histological Examination*

Histological analyses were performed after laser stimulation experiments to evaluate stimulating safety. CN was removed right after animal death and kept in 4% paraformaldehyde for 48 h. Then, the tissues were dehydrated in increasing concentrations of ethanol and were embedded in paraffin before cutting. CN tissues were cut with cross-sections (4-μm thick) on a paraffin slicing machine (RM2016, Shanghai Leica Instruments Factory, Shanghai, China). CN slices were stained with Mayer's hemotoxylin and Putt's eosin (H&E, Servicebio, China), and the CN cell status was observed under the microscope.

2.8 *Data Analysis and Statistics*

All data were analyzed offline in MATLAB 2012b (MathWorks, Inc., Natick, Massachusetts) and OriginPro 8 (OriginLab Corporation, Northampton, Massachusetts). Peristimulus time histograms (PSTHs), average firing rate, FSL, and FR change were used to analyze the neural response. The data of 50 ms after the start of each optical stimulus were used to calculate the PSTHs (25 bins/50 ms). FSL was defined as the time difference between the onset of a stimulus and the occurrence time of the first spike. The FR changes of the group of acoustical and optical co-stimulation were calculated by Eq. (4):

$$\text{FR change}\,(\%) = [\text{FR}_{(\text{A+O})} - \text{FR}_{(\text{A})}]/\text{FR}_{(\text{A})}, \tag{4}$$

where $\text{FR}_{(\text{A})}$ and $\text{FR}_{(\text{A+O})}$ represent the average FR before and after the onset of laser pulse, respectively.

The FR changes of the group of acoustical stimulation were calculated by Eq. (5):

$$\text{FR change}\,(\%) = [\text{FR}_{(\text{A1})} - \text{FR}_{(\text{A})}]/\text{FR}_{(\text{A})}, \tag{5}$$

where $\text{FR}_{(\text{A})}$ and $\text{FR}_{(\text{A1})}$ represent the average FR before the onset of laser pulse and the laser pulse is turned off, respectively.

The paired sample's t-test and analysis of variance (ANOVA) were used to do statistical analysis. Data are shown in mean and standard deviation (mean $\pm$ SD). Significance is labeled as ns ($p > 0.05$), * ($p < 0.05$), ** ($p < 0.01$), and *** ($p < 0.001$).

3 Results

3.1 *Simulation Result of Temperature Changes Under Different Laser Parameters*

Simulation diagram is shown in Fig. 2(a). The width of the model is 3 mm, the thickness is 1.1 mm, and the irradiation radius of the laser is 0.1564 mm. The tissue temperature spatial distributions of two lasers at the maximum temperature level are shown in Figs. 2(b) and 2(c). Compared with 1850 nm, 980 nm does have deep penetration in tissue, but it needs nearly 15 times more radiant energy than 1850 nm laser to achieve the same tissue baseline temperature increase.

The tissue temperature changes under different radiant energy of 980-nm laser are shown in Fig. 3. Tissue temperature increased monotonously with the increasing of the laser pulse power (pulse width: 5 ms) and pulse width (pulse power: 6 W) [see Figs. 3(a) and 3(b)]. A typical temperature rise curve over time is shown in Fig. 3(c); the laser radiant exposure was 39.06 J/cm^2 (pulse power: 6 W, pulse width: 5 ms). The curve shows that the rise time of tissue temperature was longer than the pulse width, and the time difference (δt) was about 3.4 ms. The time difference became larger when the laser pulse width was getting longer [Fig. 3(d)]. To achieve stable neural inhibition, the appropriate temperature increment induced by laser should be around 8°C.[16,32] Corresponding to our simulation result, the appropriate pulse power is about 7 W, and pulse width is about 5 ms. Considering our laser output power limitations (maximum pulse power: 6 W), pulse power in the following experiments ranged from 1 to 6 W and pulse width was from 1 to 5 ms. The corresponding radiant exposures ranged from 6.51 to 39.06 J/cm^2 at pulse width of 5 ms.

3.2 In Vivo *Study on Neuromodulation by SW-NIR*

Twelve SD rats were used in this study. ABR was performed to evaluate the hearing sensitivity of rats before and after surgery. Animals with hearing threshold under 30 dB SPL and elevated not more than 10 dB SPL after surgery were used in the following experiment. Data from 10 animals were used in the following analysis.

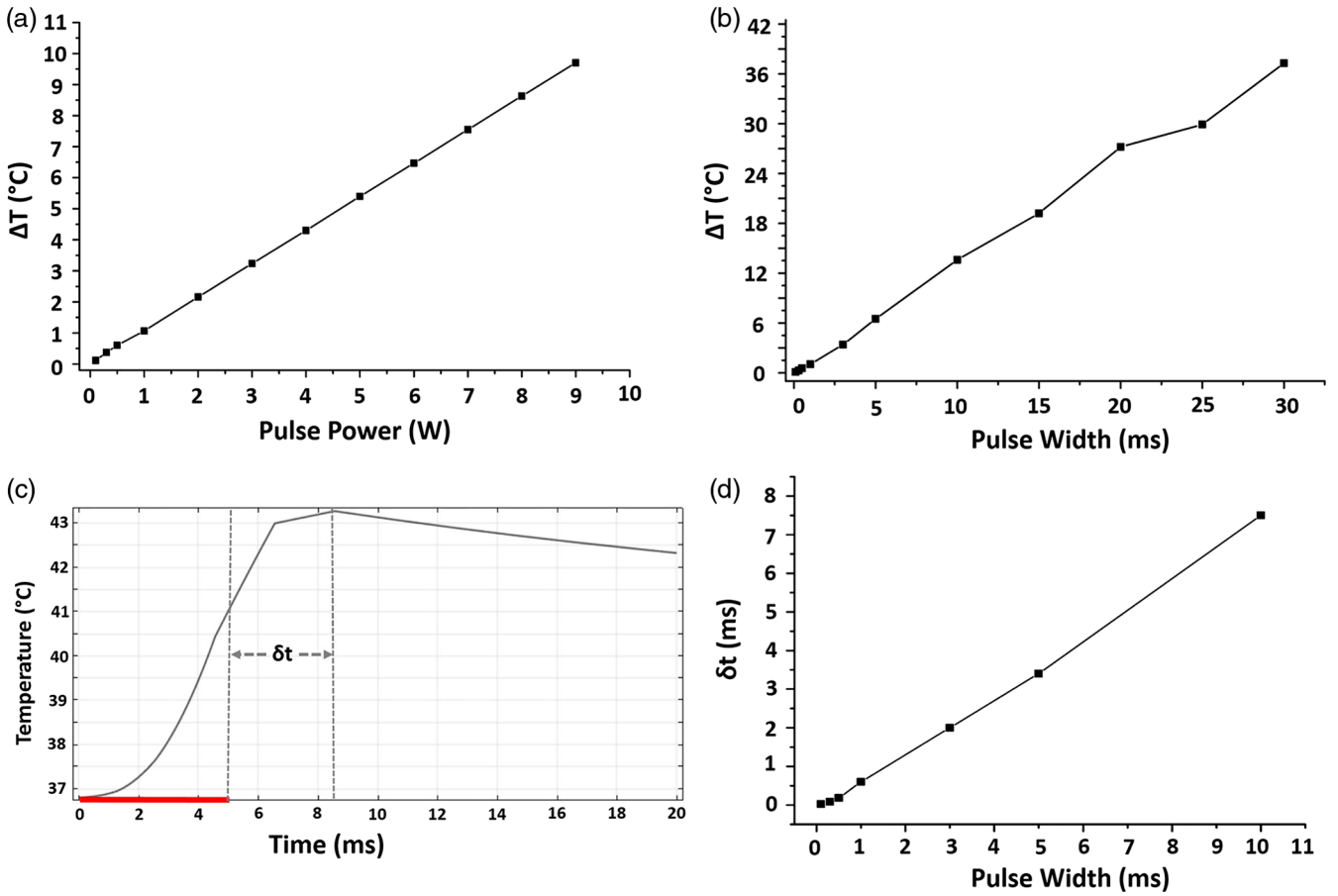

Fig. 3 Temperature changes at different stimulation parameters. Temperature changes at (a) across different laser pulse power (0.1 to 9 W, pulse width: 5 ms) and (b) different pulse width (0.1 to 30 ms, pulse power: 6 W); (c) typical temperature rise over time at radiant exposures of 39.01 J/cm^2 (pulse width: 5 ms); (d) time difference among different pulse width (0.1 to 10 ms, pulse power: 6 W). The red bar in (c) indicates an optical pulse with 5-ms pulse width.

For each animal, neural activity induced by pure tones was recorded in the IC, and CF of each neuron was calculated off-line. The CF was defined as the frequency at which the neuron is most sensitive. Neurons with a clear CF were used in the following experiments and others were rejected. Figure 4 shows the neural responses recorded one-time by a 16-channel electrode array. Each panel represents a neural response to pure tones at different pure-tone frequencies and different sound levels at one channel. The CF of neuron and electrode channel number was marked on each panel. The CFs of the recorded neurons ranged from 8 to 29.34 kHz. A total of 60 neurons were recorded in the IC of 10 SD rats. The CFs of these neurons are shown in Table 3. We mainly focused on high-frequency neurons in IC (CF more than 16 kHz) since the neurons with high CF were mostly located in dorsal cochlear nucleus (DCN), which corresponded to the site of laser irradiation.

3.2.1 *Effect of different laser parameters on acoustically induced CN neural activity*

To fix the stimulation position, we divided the surface of the DCN into nine regions [see Fig. 5(a)]. Six IC neurons with different CFs were selected as examples to show the inhibitory effect of SW-NIR. The laser radiant exposure was 39.06 J/cm^2 (pulse width: 5 ms). Figure 5(b) shows a typical response of an IC neuron before and after laser stimulation. The FR of acoustically induced neural responses [data between 12 and 14 ms are shown in Fig. 5(b)] could reach up to 400 spikes/s [Fig. 5(b), row 1] and dropped to 10 spikes/s when the laser was turned on [Fig. 5(b), row 2]. This inhibitory effect of SW-NIR could also be found on other neurons with different CFs [see Fig. 5(c)]. The FR change was about 70% (t-test, $p < 0.001$) on average [see Fig. 5(d)].

Figure 6(a) shows the inhibitory effect of SW-NIR on continuous interval neural activity induced by acoustical stimuli. The laser radiant exposure was 39.06 J/cm^2 (pulse width: 5 ms) and the stimulation frequency was 4 Hz. Before the laser was turned on, acoustic stimuli could effectively activate auditory pathway. When the laser was turned on, the acoustically induced neural activities in CN were inhibited, leading to the obviously decreased FR of IC neurons. After laser was turned off, the neuron FR quickly recovered to the initial level. The same results could be found in other neurons with different CFs [see Fig. 6(b)], which indicates that the inhibition is reversible.

The effect of different laser parameters on neurons was investigated, and results are shown in Fig. 7. First, the pulse width of stimulation was set to 5 ms, and laser pulse power from distal end of the optical fiber was adjusted from 1 to 6 W. The radiant exposures were ranging from 6.51 to 39.06 J/cm^2. Figure 7(a) shows an example of laser induced neural inhibition. The inhibitory effect enhanced with the increase of laser radiant exposures (pulse width: 5 ms). The averaged result is shown in Fig. 7(b).

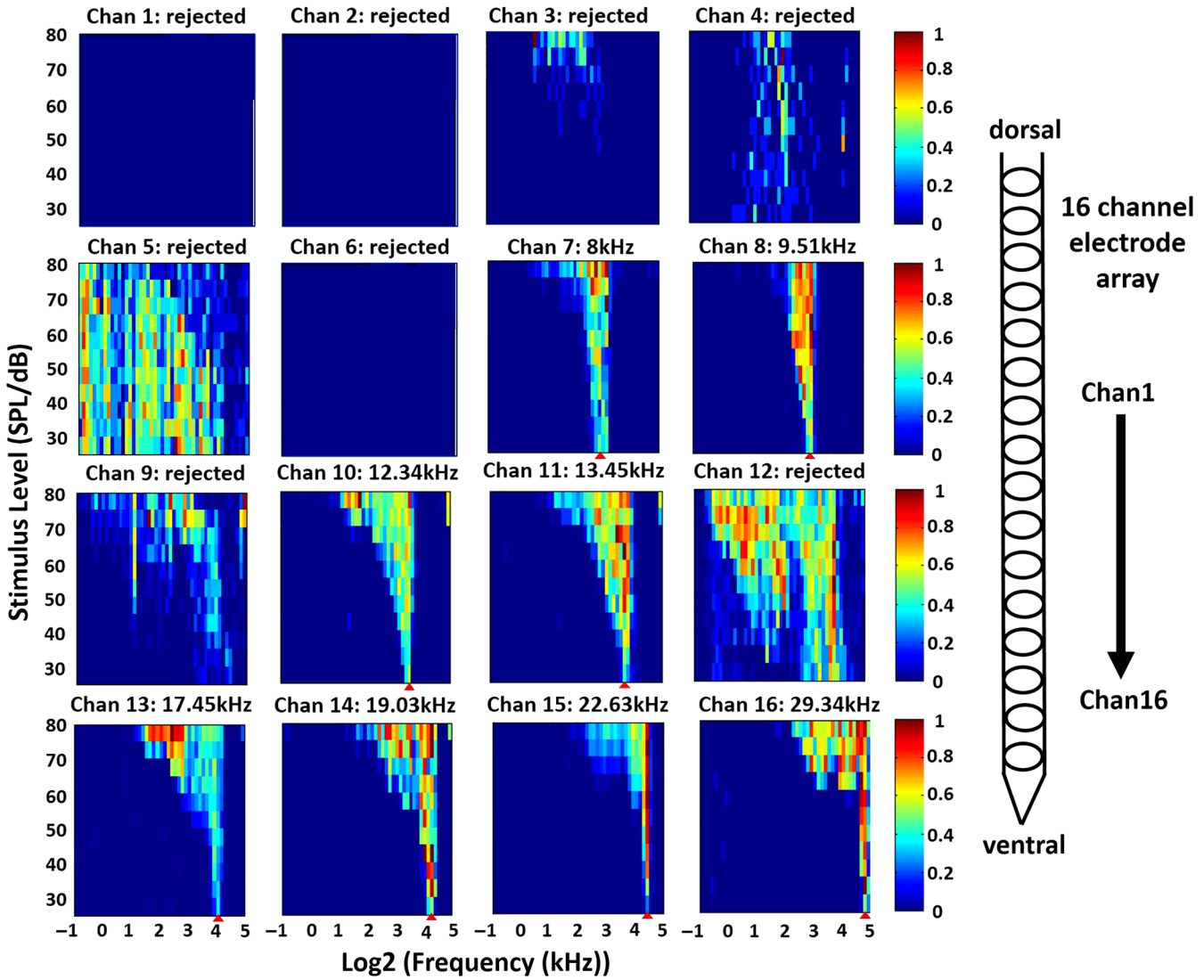

Fig. 4 Neural activity recorded in the IC in response to acoustic stimulation. Response area was normalized by its maximum FR in the area. Color indicates normalized firing rate. CF in each panel is marked as the red solid triangles. The right side is a 16-channel electrode array diagram (from top to bottom corresponding channel 1 to channel 16).

Table 3 The neural CF distribution for 60 neurons.

CF range (kHz)	0.5–8	8–16	16–22	22–32
No. of neurons	7	17	8	28

The inhibition rate increases from 20% to 71.5% when laser radiant exposures varied from 6.51 to 39.06 J/cm^2. Then, the pulse power was set to 6 W, and the pulse width was tested at 1, 3, and 5 ms, respectively. The inhibition rate increased from 54.2% to 71.5% when laser pulse width varied from 1 to 5 ms [see Fig. 7(c)].

3.2.2 *Effect of SW-NIR on neural FSL*

FSL has been found to provide more information than interval spikes, which is very important for neural temporal coding, especially in sensory systems.[43,44] Thus, we further explored laser-induced FSL changes in IC neuron. Figure 8(a) shows an example of FSL shifts before and after the laser with the radiant exposure of 39.06 J/cm^2 (pulse width: 5 ms) was turned on. The FSL of the IC neurons was obviously lengthened after the laser was turned on. Figure 8(b) shows the change of FSL for IC neurons with different CFs before and after the laser irradiation with the radiant exposure of 39.06 J/cm^2 (pulse width: 5 ms). Figure 8(c) shows the averaged lengthened time difference of FSL for IC neurons under different laser radiant exposures. The larger the laser radiant exposures (pulse width: 5 ms), the longer the lengthened time difference of FSL. The FSL lengthened from 0.7 to 4.0 ms when the laser radiant exposures raised from 6.51 to 39.06 J/cm^2 (pulse width: 5 ms). The same trend was also obtained under different laser pulse widths [see Fig. 8(d)]. The FSL lengthened from 3.3 to 4.0 ms when laser pulse width was changed from 1 to 5 ms (pulse power: 6 W).

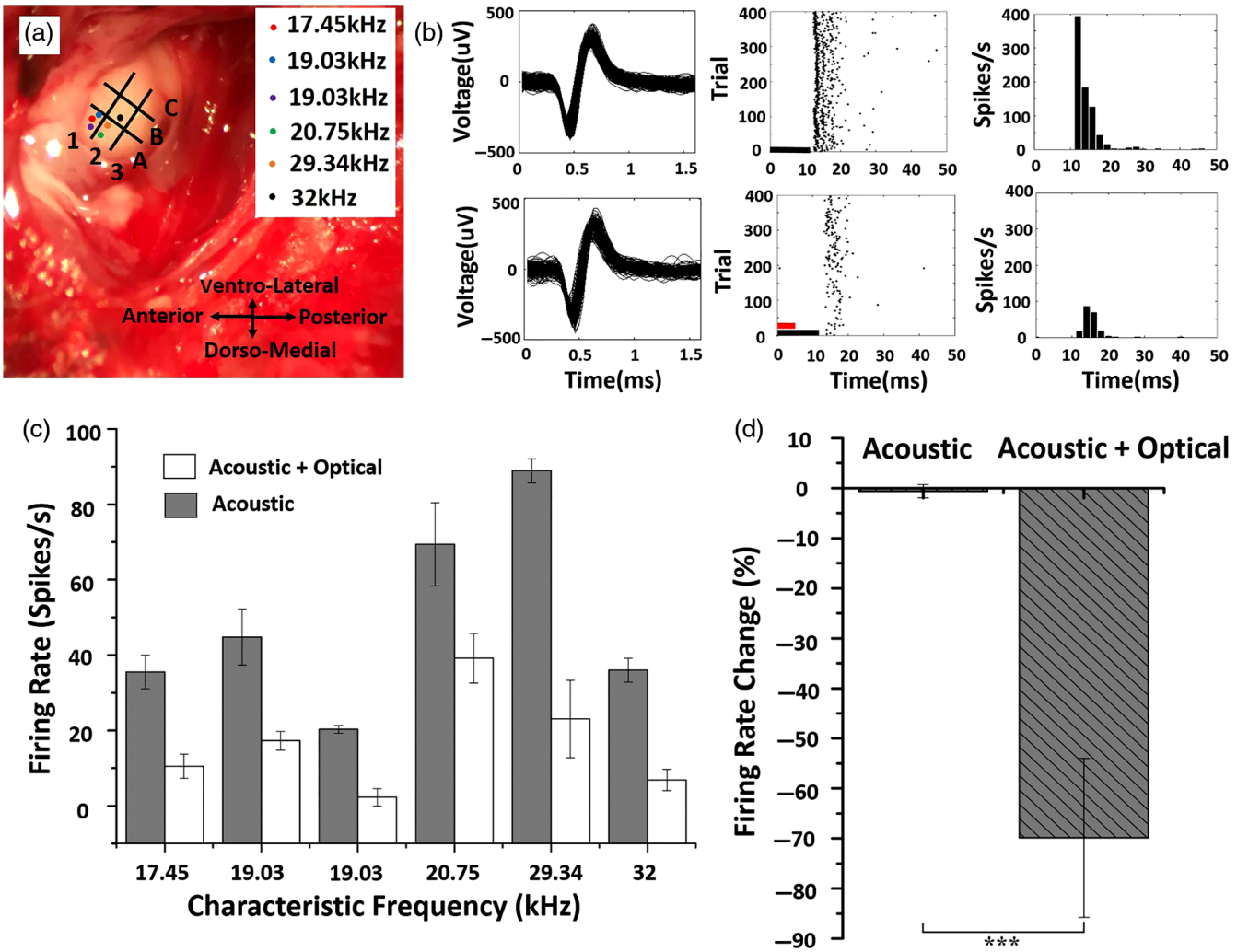

Fig. 5 The inhibitory effect of SW-NIR on acoustically induced neural activities in CN. (a) Nine partitions and stimulating points were marked on the surface of DCN. (b) The effect of SW-NIR on the spikes FR of IC neurons with the radiant exposure of 39.06 J/cm^2 (pulse width: 5 ms, pure tone frequency: 19.03 kHz, sound level: 80 dB SPL). The first row: IC neurons response to acoustic stimuli, the second row: IC neurons response to optical and acoustical co-stimulation. From left to right were neuron waveforms plots, neuron raster plots and PSTH. The black line and red line in the second column indicate the stimulation duration of acoustic (12 ms) and optical (5 ms) stimulus, respectively. (c) The effect of SW-NIR with the radiant exposure of 39.06 J/cm^2 on spikes FR of IC neurons with different CFs (pulse width: 5 ms, trials: 400). (d) Averaged FR change of IC neurons were affected by SW-NIR with the radiant exposure of 39.06 J/cm^2 (pulse width: 5 ms, *t*-test, $p < 0.001$, No. of neurons: 6, trials: 400). The values represent mean ± SD.

3.2.3 *Effect of different stimulation paradigms on acoustically induced CN neural activity*

Four different stimulation paradigms used in this study are shown in Fig. 9(a) (the first row). In each stimulation paradigm, pure tone with a fixed frequency (neuron CF) was used to stimulate from external auditory canal. The laser radiant exposure was 39.06 J/cm^2 (pulse width: 5 ms). Figure 9(a) shows IC neurons in response to four stimulation paradigms. Neural inhibitory rates under different stimulation paradigms were summarized in Fig. 9(b). One-way ANOVA showed that the effect of stimulation paradigms on the neural FR change was significant. And the largest inhibition occurred when the laser pulse was prior and synchronous to the acoustical stimulus (Fig. 9). Compared with acoustic and optical synchronous stimulation, optical prior to acoustic stimulus could obtain a higher inhibitory rate (67.4% versus 87.5%) (ANOVA, $p = 0.046$). Similar results were obtained in the neural FSL statistics [see Fig. 9(c)]. This may result from the establishment time of the tissue temperature field induced by laser pulse. From our simulation result, we could see that tissue temperature rising time was longer than laser pulse width. With the first stimulation paradigm, tissue temperature rose to a higher level when the neural signal transmitted to CN, so the inhibition effect of laser on CN neuron was better than other stimulation paradigms.

3.3 *Histology of SW-NIR in CN*

Histological analysis of DCN was carried out after the experiment to verify the safety of SW-NIR. Results are shown in Fig. 10. The negative control group was given fake laser

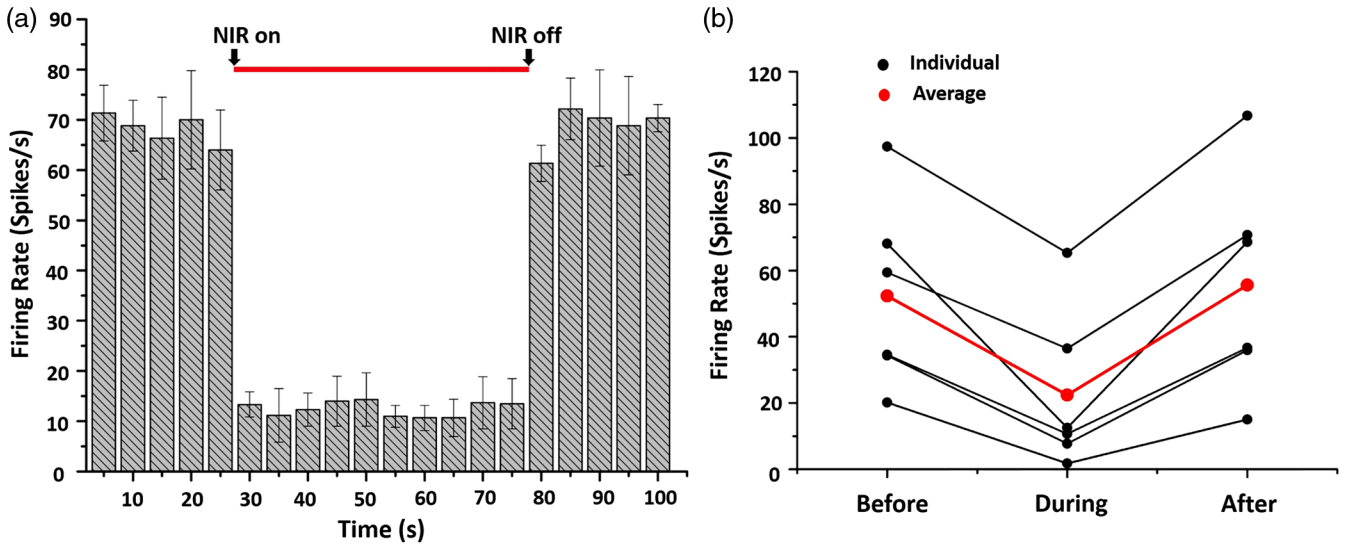

Fig. 6 The inhibitory effect of SW-NIR on continuous neural activity induced by acoustical stimuli. (a) An example of laser-induced reversible inhibition on acoustically induced neural activity with the radiant exposure of 39.06 J/cm^2 (pulse width: 5 ms). The red line indicates SW-NIR with 50-s irradiation. The values represent mean ± SD. (b) The effect of the spikes FR of IC neurons with different CFs before and after laser stimulation with the radiant exposure of 39.06 J/cm^2 (pulse width: 5 ms). The black and red points represent individual neurons and the average firing rate, respectively.

stimulation (laser off), the experimental group was given radiant exposure of 39.06 J/cm^2 (pulse width: 5 ms).

The irradiation position on the DCN and slice cutting orientation was shown in Fig. 10(a). Based on anatomical structure, we can find the edges of the CN [blue dash line in Fig. 10(a)], and the two edges of CN served as reference lines [also see red triangles in Fig. 10(d)]. After we found the reference lines, we stimulated CN along the middle line of CN [red dash line in Fig. 10(a)]. Then, we cut the tissue as 4-μm thick slices parallel with the black line of the Fig. 10(a) during the histology staining. Thus, the center between two edges of every slice is the stimulation site [red dash line in Fig. 10(a) and red dashed rectangle in Figs. 10(d)–10(f)]. Compared with negative control groups [Figs. 10(b)–10(c)], no tissue damage was found in our experimental group [Figs. 10(d)–10(f)], which indicated that no irreversible damage occurred to the CN tissues during the stimulation experiment.

4 Discussion

The present study demonstrated that SW-NIR with a wavelength of 980 nm could reversibly inhibit the CN neural activities induced by acoustical stimuli, and block the transmission of neural signals to the higher level of the central nervous system consequently. Under the laser parameters used in this experiment, the higher the laser pulse power, the more significant the inhibition effect. And the largest inhibitory effect on CN neurons could be observed when laser pulse was prior to acoustical stimulus, which indicates that the inhibition relies on the establishment time of the temperature field.

4.1 *Optical Stimulation on Rat's Auditory System*

The idea of using an auditory system to study the inhibitory effect of SW-NIR on the central nervous system *in vivo* was from our previous study on auditory brainstem stimulating method based on SW-NIR.[33] In that study, we tried to use 980-nm laser pulse to activate CN neurons *in vivo*, and we occasionally found that 980-nm laser pulse could inhibit CN neural activity and cause associated IC neural FR reduction. Second, the auditory system has a specific tonotopic organization;[45] auditory nerves from different regions of the cochlea transmit tonotopically encoded sound frequency information through associated midbrain structures and finally to the primary auditory cortex. In other words, the response of IC neurons depends on the input of the dorsal and ventral CN.[46] In the auditory system, each auditory pathway has its own CF, therefore, the corresponding neurons with the same CF are relatively easily found. Moreover, IC tonotopic maps are very clear in the most mammals and were widely used to evaluate auditory responses decades ago.[27,47,48] In addition to the special tonotopic organization of the auditory pathway described above, the purpose of this experiment was to investigate how SW-NIR regulates neural activities and nerve conduction *in vivo*. Thus, we used neural responses in IC to evaluate the effect of SW-NIR on CN neural suppression and nerve conduction.

4.2 *Temperature Distribution of SW-NIR and NIR used in Neuromodulation*

Compared with NIR, the SW-NIR has a much lower absorption coefficient and stronger scattering coefficient,[41] which is less favorable for infrared neuromodulations. And if we only consider the effectiveness of neuromodulation by laser, NIRs do have better behaviors than SW-NIRs. However, when we use laser pulse to modulate neural activities or nerve conduction *in vivo*, the penetrability of laser pulse is indispensable, especially in deep brain stimulation.[2] From our simulation results, we could see that the 980-nm laser has a temperature distribution in tissue wider than 1850 nm, and it could easily reach the deeper layer neurons in tissue. Recently, it has been reported that nanoparticles could effectively enhance the stimulation efficiency and spatial resolution of laser stimulation.[49] From our result, although it needs nearly 15 times more radiant energy for 980-nm laser than 1850-nm laser to achieve the same tissue

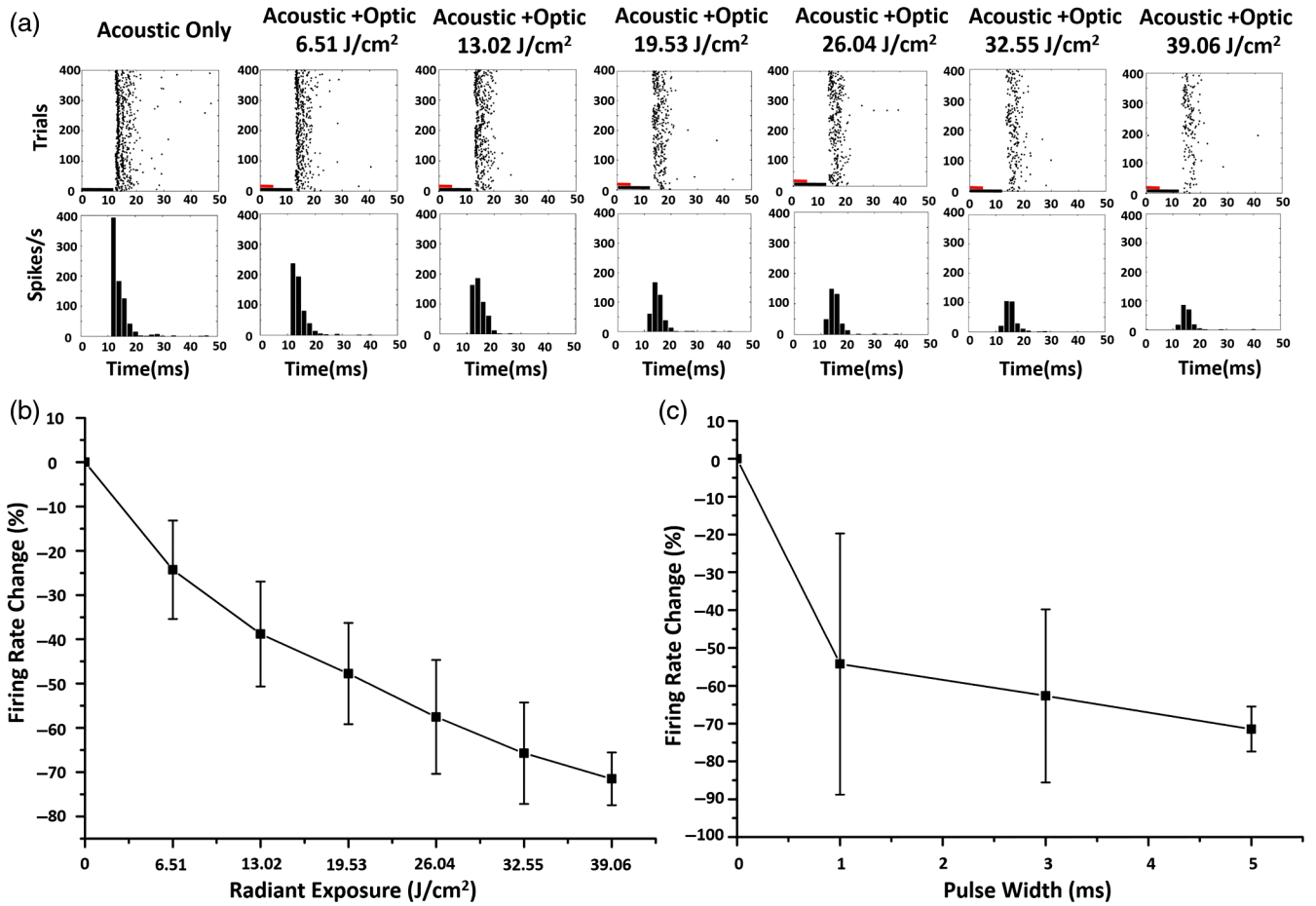

Fig. 7 The inhibitory effect of SW-NIR on acoustically induced neural activities in CN under different laser parameters. (a) An example of inhibitory effect enhanced with the increase of laser radiant exposures (pure tone frequency: 17.45 kHz, sound level: 80 dB SPL). The first row was neuron raster plots, and the second row was PSTH. The black line and red line in the corner of first indicate the stimulation duration of acoustic (12 ms) and optical (5 ms) stimulus, respectively. (b) Averaged FR change as a function of laser radiant exposures varied from 6.51 to 39.06 J/cm^2 (pulse width: 5 ms). (c) Averaged FR change as a function of laser pulse width varied from 1 to 5 ms (in 2-ms step, pulse power: 6 W). The pure tone frequencies were 17.45, 19.03, 19.03, 20.75, 29.34, and 32 kHz, respectively. The sound level was 80 dB SPL. The values represent mean ± SD.

baseline temperature increase, nanoparticles could be added into target tissue to enhance the photothermal interactions between laser and tissue, thereby reducing the laser energy and improving the targeting ability of the 980-nm laser.

Simulating results also showed that the temperature falls slowly after laser stimulation (Fig. 3), and it takes about 1.2 s for the temperature to return to the baseline (see Fig. S2 in the Supplementary Material), which exceeds the stimulation time interval (250 ms) in animal experiments and might cause temperature accumulation in tissue. However, from the existing experimental results (see Fig. 6 and Fig. S3 in the Supplementary Material), there is no obvious difference of the neural firing rate along the stimulating period, which indicates that even optical pulses may cause temperature accumulation in tissue; it did not affect the stimulation effect in this study.

4.3 *Inhibitory Effect of Optical Stimulation Parameters on CN Neurons*

The detailed mechanism of infrared neural modulation is far from clear, and the photothermal effect between laser and tissue is generally accepted as the basic mechanism.[6,16,19,20,32,50,51] Different from optically induced neural activity, the neural inhibition induced by laser pulse is based on the tissue baseline temperature rise.[16,19,20,32] Temperature changes in tissue could be controlled by adjusting laser parameters, including laser wavelength, pulse power, pulse width, repetition rate, and so on,[23,32] or by changing tissue's ability to absorb laser radiation, for instance by adding certain nanoparticles into target tissue.[16,19] This work was mainly focused on the effect of SW-NIR (wavelength of 980 nm) parameters on neural inhibition. Our results showed that with the increasing of laser radiant exposures from 6.51 to 39.06 J/cm^2 (pulse width: 5 ms), the increment temperature of the CN increased from 1°C to 6.5°C [Fig. 3(a)] and the neural inhibition rate increased from 25% to 70% [Fig. 7(b)], which is similar to the results from Yoo et al.[16] In their studies, a continuous 785-nm infrared laser was used to modulate cultured hippocampal neurons, and temperature induced by laser pulse was enhanced by adding gold nanorods into neurons. Their results showed that when the temperature rose by 2°C to 8°C, the inhibition rate varied from 40% to 89.6%. Similar results were also found in other infrared neuromodulation experiments carried out *in vitro*.[19,20]

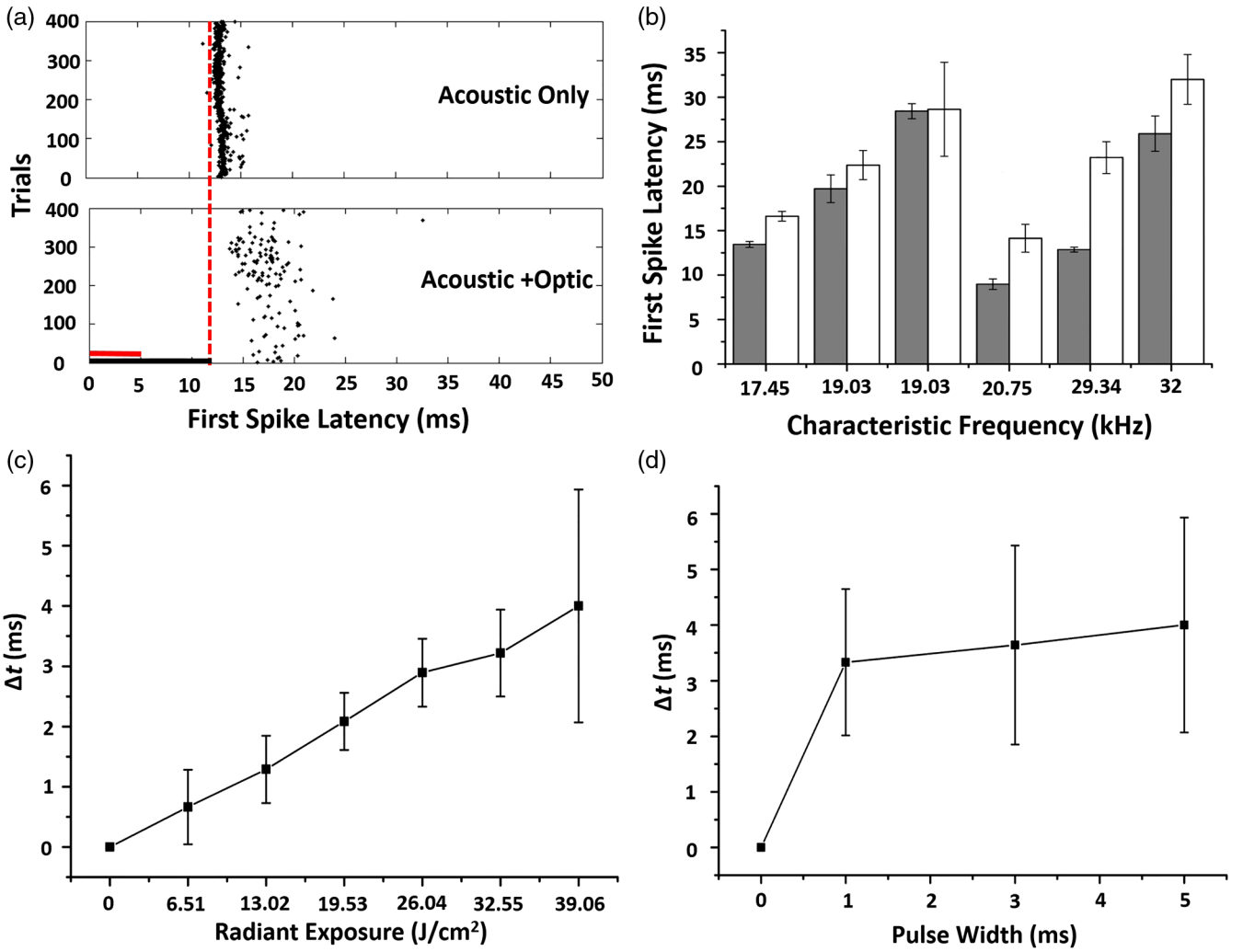

Fig. 8 The effect of SW-NIR on the FSL of IC neurons. (a) An example of SW-NIR with the radiant exposure of 39.06 J/cm^2 (pulse width: 5 ms) affect the FSL of IC neurons. The black line and red line in the second column indicate the time of acoustic (12 ms) and optical (5 ms) stimulus, respectively. (b) The effect of SW-NIR with the radiant exposure of 39.06 J/cm^2 (pulse width: 5 ms) on the FSL of IC neurons at different CFs. (c) The effect of SW-NIR on the FSL of IC neurons under different laser radiant exposures varied from 6.51 to 39.06 J/cm^2 (pulse width: 5 ms). (d) The effect of SW-NIR on the FSL of IC neurons at different laser pulse width varied from 1 to 5 ms (in 2-ms step, pulse power: 6 W). The values represent mean ± SD.

With the increase of our laser pulse width (pulse power: 6 W), the inhibition rate increased from 54.2% to 72.5%. Although the change was slight, the inhibition became more stable with larger pulse width [Fig. 7(c)], which may also be related to tissue baseline temperature induced by SW-NIR. For infrared neuromodulation, laser parameters are always limited by a maximum temperature that neural tissue can withstand, which is also known as the tissue ablation threshold.[52,53] Beyond this threshold, tissue will be thermally ablated. According to previous studies, this threshold is about 56°C.[52] Our simulation result showed that the longer the pulse duration, the higher the tissue temperature induced. When the optical parameter was set to 6-W pulse power and 14-ms pulse width and the corresponding radiant exposure was 109.37 J/cm^2, the CN temperature rose about 55°C, which is very close to the ablation threshold. To avoid nerve tissue damage, we only focused on the shorter pulse width of SW-NIR.

4.4 *Effect of SW-NIR on Neural FSL*

Studies showed that temporal codes based on FSL contain more information, which is important for the study of neural coding mechanisms.[47,54] In the auditory system, it has been suggested that FSL may represent auditory features, such as signal amplitude, frequency, and threshold, more accuracy than the neural FR.[43,44,55,56] And FSL was more sensitive to the most stimuli.[43,44] Here, we explored laser-induced FSL changes in IC neuron. We found that SW-NIR does affect neural FSL in our experiment. The neural FSL was longer when the laser pulse energy was larger [Figs. 8(c) and 8(d)]. Studies demonstrated that the change of neural FSL may relate to any factors that affects nerve conduction.[57] In this study, nerve conduction was modulated by temperature deposited in CN. With the increasing of laser pulse energy, more radiation energy was absorbed by CN neurons, followed by the tissue baseline temperature

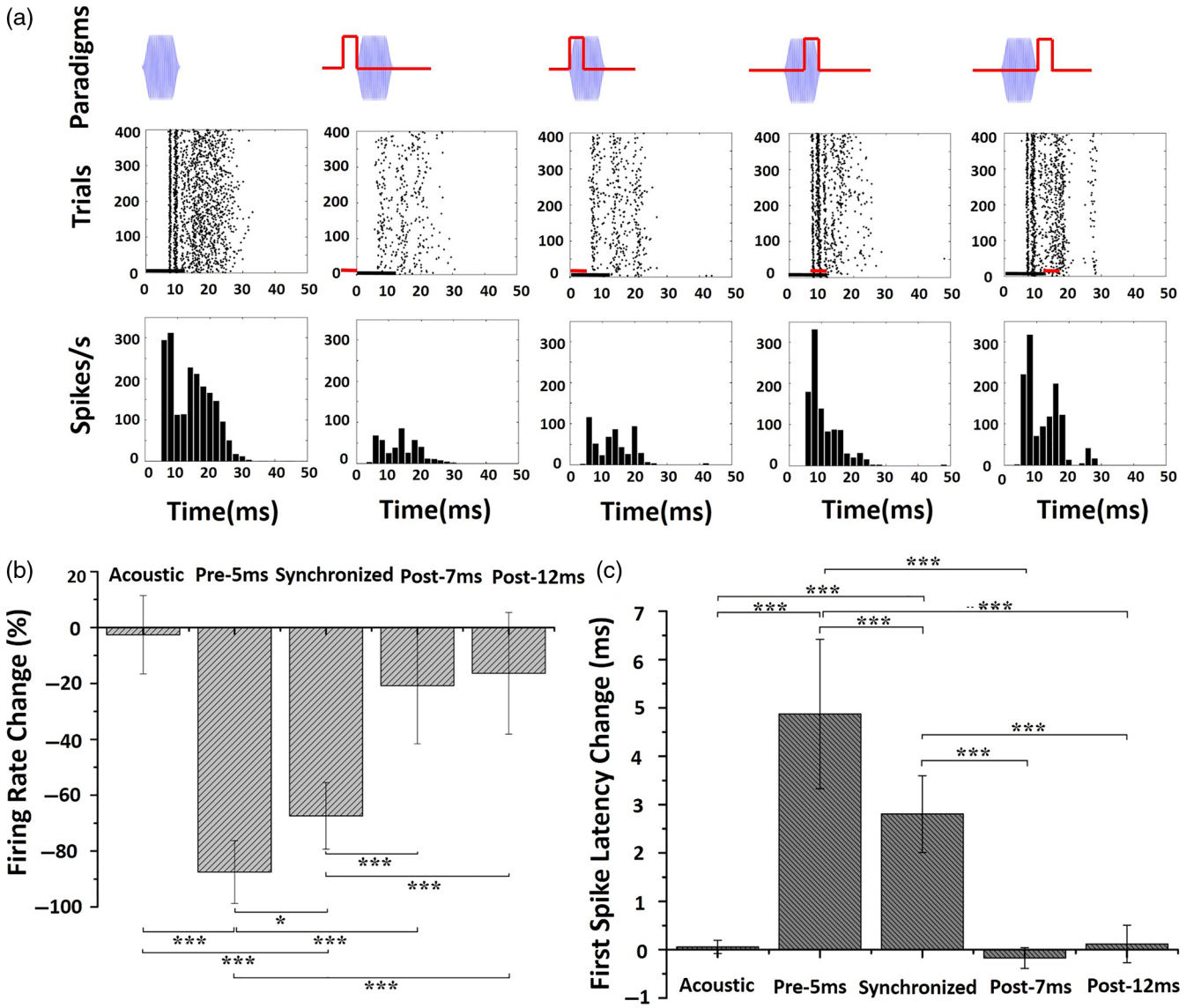

Fig. 9 The inhibitory effect of optical stimulation on acoustically induced neural activities in CN under different stimulation paradigms. (a) The neural responses under four stimulation paradigms. The first row was four stimulation paradigm types, the second row was neuron raster plots corresponding to each stimulation paradigm, and the third row was PSTH. (b) FR changes and (c) FSL of IC neurons in the optical stimulation under different stimulation paradigms, significant differences were shown between groups. The values represent mean ± SD.

increasing, which inhibited the neural activity and nerve conduction, and finally caused the prolonged neural FSL. Meanwhile, we found that the neural FSL varied greatly from neurons with different CFs [Fig. 8(b)], this was mainly caused by different neural transmitting pathways among different neurons between IC and DCN. Similar results can be found in previous studies.[47]

4.5 *Inhibitory Effect of Different Stimulation Paradigms on CN Neurons*

Four stimulation paradigms were investigated in this study, and results showed that optical stimulus prior and synchronous to acoustical stimulus could effectively inhibit the acoustically induced neural activities of CN neurons. Optical stimulus delivered 5 ms prior to acoustic stimulus had the most significant inhibitory effect on CN neurons [Figs. 9(b) and 9(c)]. This is mainly related to the establishment time of tissue temperature field. Optically induced tissue temperature increase is not a kind of instantaneous action but a process.[32] The simulation result showed that the tissue temperature reached the highest level, 3.4 ms, after the end of the optical stimulus with the radiant exposure of 39.06 J/cm^2 (pulse width: 5 ms) [Fig. 3(c)]. The larger the pulse width, the longer the time difference [Fig. 3(d)]. Duke et al. also recorded similar results from sciatic nerve of rat's peripheral pathway.[32] Under the first stimulation paradigm, tissue temperature reaches the highest level when CN neurons were about to be activated by acoustical stimuli, thus the inhibitory effect was significant. In other stimulation paradigms, neural tissue temperature was relatively low so that the inhibitory effect on CN neurons was relatively poor. This result further demonstrates that the level of tissue baseline

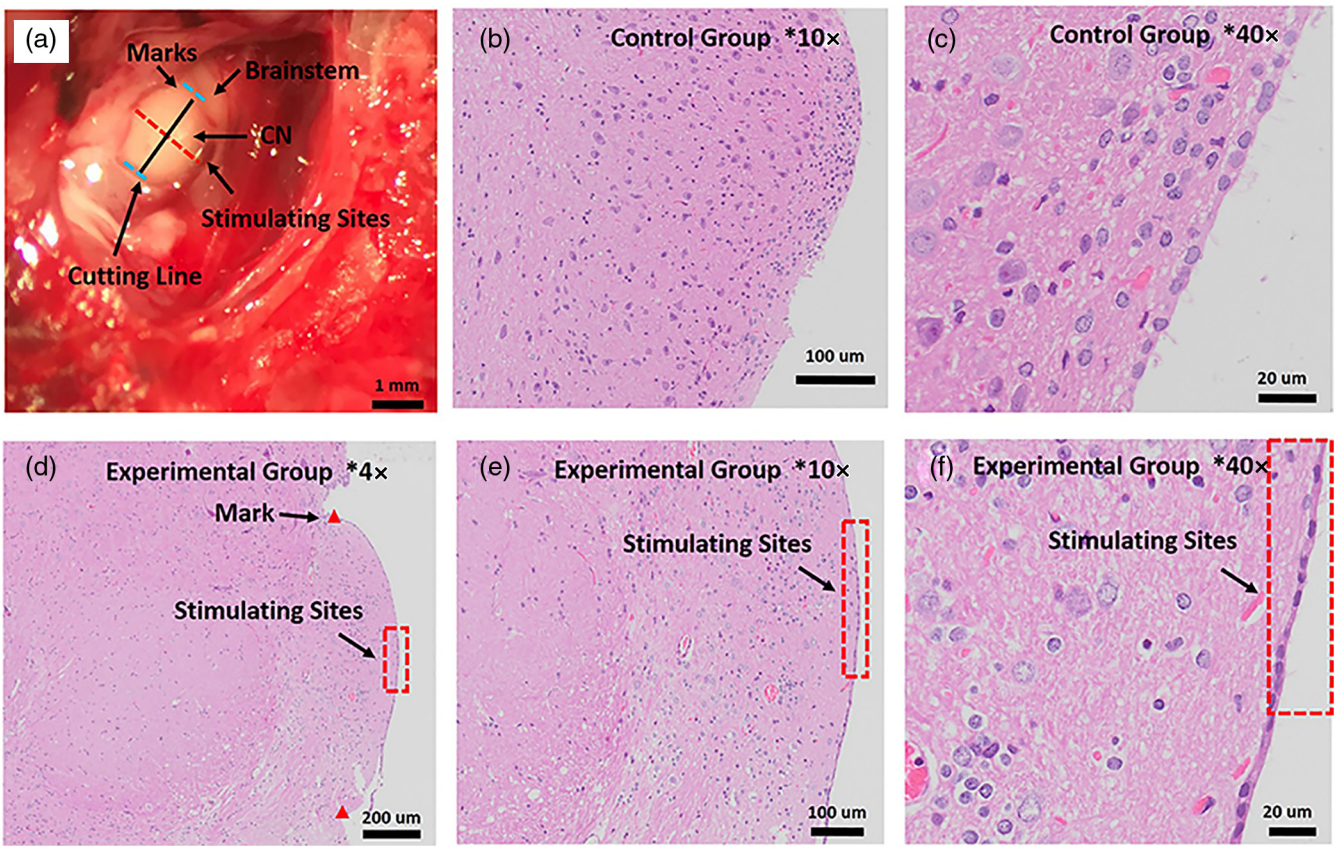

Fig. 10 Safety analysis of DCN exposed to laser irradiation. (a) The position of stimulating sites, the orientation of slice cutting line, and the position of marks. (b) and (c) Magnified view of negative control group, taken with a 10×, 40× objective. (d)–(f) Magnified view of experimental group, photographed using a 4×, 10×, 40× objective. The tissue irradiated with the radiant exposure of 39.06 J/cm^2 (pulse width: 5 ms). The solid red triangles were marks. The red dashed rectangles were stimulating sites.

temperature is the main factor for infrared neural inhibition and the neural inhibition relies on the establishment time of temperature field.

5 Conclusion

In this paper, we first introduced SW-NIR with the wavelength of 980 nm into neuromodulation in the central nervous system *in vivo*. Both stimulation parameters and stimulation paradigms of SW-NIR were investigated on the rat's central auditory system. The study showed that 980-nm laser pulses could reversibly and repeatedly inhibit acoustically induced neural activities in CN, and that the inhibition relies on the establishment time of the tissue temperature field. Moreover, our preliminary results suggest that short-wavelength infrared could regulate the activities of neurons beyond the neural tissues laser irradiated through neural networks and conduction *in vivo*. Based on the above experimental results, a type of neuromodulation tool with a transcutaneous stimulation mode is quite promising. This may be of great importance for improving the treatment of neurological disorders, such as epilepsy, tinnitus, neuropathic pain, and Parkinson's disease. Further work will focus on the study of precise transcutaneous stimulation methods *in vivo* using SW-NIR; temperature accumulation induced by laser pulse will be tested and the stimulus parameters will be readjusted in the follow-up experiments.

Disclosures

The authors have no additional relevant financial interests or potential conflicts of interest.

Acknowledgments

This work was supported by the National Natural Science Foundation of China (Grant Nos. 31271060, 31700855, 31700856, and 31872751); the Natural Science Foundation of Chongqing, China (Grant No. cstc2015jcyjBX0101); Shandong Provincial Natural Science Foundation, China (Grant No. ZR2017BC041); and the Visiting Scholar Foundation of Key Laboratory of Biorheological Science and Technology (Chongqing University), Ministry of Education (Grant No. CQKLBST-2017-004).

References

1. D. Zumsteg, A. M. Lozano, and R. A. Wennberg, "Depth electrode recorded cerebral responses with deep brain stimulation of the anterior thalamus for epilepsy," *Clin. Neurophysiol.* **117**(7), 1602–1609 (2006).
2. J. M. Encinas et al., "Neurogenic hippocampal targets of deep brain stimulation," *J. Comp. Neurol.* **519**(1), 6–20 (2011).
3. A. W. Laxton et al., "A phase I trial of deep brain stimulation of memory circuits in Alzheimer's disease," *Ann. Neurol.* **68**(4), 521–534 (2010).
4. W. M. Grill, S. E. Norman, and R. V. Bellamkonda, "Implanted neural interfaces: biochallenges and engineered solutions," *Annu. Rev. Biomed. Eng.* **11**, 1–24 (2009).

5. A. R. Duke et al., "Spatial and temporal variability in response to hybrid electro-optical stimulation," *J. Neural Eng.* **9**(3), 036003 (2012).
6. J. Wells et al., "Pulsed laser versus electrical energy for peripheral nerve stimulation," *J. Neurosci. Methods* **163**(2), 326–337 (2007).
7. A. D. Izzo et al., "Laser stimulation of the auditory nerve," *Lasers Surg. Med.* **38**(8), 745–753 (2006).
8. J. M. Cayce et al., "Infrared neural stimulation of thalamocortical brain slices," *IEEE J. Sel. Top. Quant. Electron.* **16**(3), 565–572 (2010).
9. J. M. Cayce et al., "Infrared neural stimulation of primary visual cortex in non-human primates," *Neuroimage* **84**, 181–190 (2014).
10. J. M. Cayce et al., "Pulsed infrared light alters neural activity in rat somatosensory cortex in vivo," *Neuroimage* **57**(1), 155–166 (2011).
11. X. D. Tan et al., "Auditory neural activity in congenitally deaf mice induced by infrared neural stimulation," *Sci. Rep.* **8**, 388 (2018).
12. H. K. Young et al., "Target structures for cochlear infrared neural stimulation," *Neurophotonics* **2**(2), 025002 (2015).
13. M. Chernov and A. W. Roe, "Infrared neural stimulation: a new stimulation tool for central nervous system applications," *Neurophotonics* **1**(1), 011011 (2014).
14. B. Entwisle et al., "In vitro neuronal depolarization and increased synaptic activity induced by infrared neural stimulation," *Biomed. Opt. Express* **7**(9), 3211–3219 (2016).
15. J. L. Carvalho-de-Souza et al., "Photosensitivity of neurons enabled by cell-targeted gold nanoparticles," *Neuron* **86**(1), 207–217 (2015).
16. S. Yoo et al., "Photothermal inhibition of neural activity with near-infrared-sensitive nanotransducers," *ACS Nano* **8**(8), 8040–8049 (2014).
17. F. Zhang et al., "Multimodal fast optical interrogation of neural circuitry," *Nature* **446**(7136), 633–639 (2007).
18. K. L. Kilgore and N. Bhadra, "Nerve conduction block utilising high-frequency alternating current," *Med. Biol. Eng. Comput.* **42**(3), 394–406 (2004).
19. J. W. Lee et al., "Gold nanostar-mediated neural activity control using plasmonic photothermal effects," *Biomaterials* **153**, 59–69 (2018).
20. S. Yoo et al., "Electro-optical neural platform integrated with nanoplasmonic inhibition interface," *ACS Nano* **10**(4), 4274–4281 (2016).
21. Z. X. Mou et al., "A simulation study of the combined thermoelectric extracellular stimulation of the sciatic nerve of the xenopus laevis: the localized transient heat block," *IEEE Trans. Biomed. Eng.* **59**(6), 1758–1769 (2012).
22. E. H. Lothet et al., "Alternating current and infrared produce an onset-free reversible nerve block," *Neurophotonics* **1**(1), 011010 (2014).
23. E. H. Lothet et al., "Selective inhibition of small-diameter axons using infrared light," *Sci. Rep.* **7**, 3275 (2017).
24. A. J. Walsh et al., "Action potential block in neurons by infrared light," *Neurophotonics* **3**(4), 040501 (2016).
25. A. D. Izzo et al., "Laser stimulation of auditory neurons: effect of shorter pulse duration and penetration depth," *Biophys. J.* **94**(8), 3159–3166 (2008).
26. G. M. Hale and M. R. Querry, "Optical constants of water in the 200-nm to 200-um wavelength region," *Appl. Opt.* **12**, 555–563 (1973).
27. N. Xia et al., "Pulsed 808-nm infrared laser stimulation of the auditory nerve in guinea pig cochlea," *Lasers Med. Sci.* **29**(1), 343–349 (2014).
28. J. X. Wang et al., "Effect of shorter pulse duration in cochlear neural activation with an 810-nm near-infrared laser," *Lasers Med. Sci.* **32**(2), 389–396 (2017).
29. J. X. Wang et al., "Pulsed 980 nm short wavelength infrared neural stimulation in cochlea and laser parameter effects on auditory response characteristics," *Biomed. Eng. Online* **14**, 89 (2015).
30. L. Tian et al., "Short-wavelength infrared laser activates the auditory neurons: comparing the effect of 980 vs. 810 nm wavelength," *Lasers Med. Sci.* **32**(2), 357–362 (2017).
31. M. Q. Wang et al., "Optical stimulation of primary motor cortex with 980 nm infrared neural stimulation," in *36th Annu. Int. Conf. IEEE Eng. Med. and Biol. Soc. (EMBC)*, pp. 6143–6146 (2014).
32. A. R. Duke et al., "Transient and selective suppression of neural activity with infrared light," *Sci. Rep.* **3** (2013).
33. B. Jiang et al., "Auditory responses to short-wavelength infrared neural stimulation of the rat cochlear nucleus," in *39th Annu. Int. Conf. IEEE Eng. Med. and Biol. Soc. (EMBC)*, pp. 1942–1945 (2017).
34. D. McFadden, "Sex differences in the auditory system," *Dev. Neuropsychol.* **14**(2–3), 261–298 (1998).
35. G. H. Lu, T. Maekawa, and H. Kimura, "An integrated model of thermodynamic-hemodynamic-pharmacokinetic system and its application on decoupling control of intracranial temperature and pressure in brain hypothermia treatment," *J. Theor. Biol.* **242**(1), 16–31 (2006).
36. Y. Shin et al., "Characterization of fiber-optic light delivery and light-induced temperature changes in a rodent brain for precise optogenetic neuromodulation," *Biomed. Opt. Express* **7**(11), 4450–4471 (2016).
37. D. A. Nelson and S. A. Nunneley, "Brain temperature and limits on transcranial cooling in humans: quantitative modeling results," *Eur. J. Appl. Physiol. Occup. Physiol.* **78**(4), 353–359 (1998).
38. H. H. Pennes, "Analysis of tissue and arterial blood temperatures in the resting human forearm," *J. Appl. Physiol.* **1**(2), 93–122 (1948).
39. A. J. Welch, "The thermal response of laser irradiated tissue," *IEEE J. Quant. Electron.* **20**(12), 1471–1481 (1984).
40. T. Li et al., "Photon penetration depth in human brain for light stimulation and treatment: a realistic Monte Carlo simulation study," *J. Innov. Opt. Health Sci.* **10**(5), 1743002 (2017).
41. T. Myllyla et al., "Assessment of the dynamics of human glymphatic system by near-infrared spectroscopy," *J. Biophotonics* **11**(8), e201700123 (2018).
42. A. C. Thompson et al., "Modeling of the temporal effects of heating during infrared neural stimulation," *J. Biomed. Opt.* **18**(3), 035004 (2013).
43. X. D. Tan et al., "First spike latency and spike count as functions of tone amplitude and frequency in the inferior colliculus of mice," *Hear. Res.* **235**(1–2), 90–104 (2008).
44. P. Heil, "First-spike latency of auditory neurons revisited," *Curr. Opin. Neurobiol.* **14**(4), 461–467 (2004).
45. A. F. Ryan, N. K. Woolf, and F. R. Sharp, "Tonotopic organization in the central auditory pathway of the Mongolian Gerbil—a 2-deoxyglucose study," *J. Comp. Neurol.* **207**(4), 369–380 (1982).
46. B. R. Schofield, "Origins of projections from the inferior colliculus to the cochlear nucleus in guinea pigs," *J. Comp. Neurol.* **429**(2), 206–220 (2001).
47. S. J. Mauger et al., "An in vivo investigation of first spike latencies in the inferior colliculus in response to multichannel penetrating auditory brainstem implant stimulation," *J. Neural Eng.* **7**(3), 036004 (2010).
48. R. U. Verma et al., "Auditory responses to electric and infrared neural stimulation of the rat cochlear nucleus," *Hear. Res.* **310**, 69–75 (2014).
49. K. Eom et al., "Enhanced infrared neural stimulation using localized surface plasmon resonance of gold nanorods," *Small* **10**(19), 3853–3857 (2014).
50. I. U. Teudt et al., "Optical stimulation of the facial nerve: a new monitoring technique?" *Laryngoscope* **117**(9), 1641–1647 (2007).
51. C. P. Richter et al., "Optical stimulation of auditory neurons: effects of acute and chronic deafening," *Hear. Res.* **242**(1–2), 42–51 (2008).
52. J. Wells et al., "Biophysical mechanisms of transient optical stimulation of peripheral nerve," *Biophys. J.* **93**(7), 2567–2580 (2007).
53. M. M. Chernov, G. Chen, and A. W. Roe, "Histological assessment of thermal damage in the brain following infrared neural stimulation," *Brain Stimul.* **7**(3), 476–482 (2014).
54. M. N. Shivdasani et al., "Neural synchrony in ventral cochlear nucleus neuron populations is not mediated by intrinsic processes but is stimulus induced: implications for auditory brainstem implants," *J. Neural Eng.* **6**(6), 065003 (2009).
55. P. Heil, "Auditory cortical onset responses revisited. 1. First-spike timing," *J. Neurophysiol.* **77**(5), 2616–2641 (1997).
56. P. Heil et al., "Towards a unifying basis of auditory thresholds: distributions of the first-spike latencies of auditory-nerve fibers," *Hear. Res.* **238**(1–2), 25–38 (2008).
57. Z. X. Mou et al., "Pulsed near infrared laser stimulates the rat visual cortex in vivo," *Biocybern. Biomed. Eng.* **35**(4), 247–254 (2015).

Bin Jiang is a doctoral candidate majoring in biomedical engineering at Chongqing University in China. He received his bachelor's degree in biomedical engineering from Chongqing University of Technology, Chongqing, China in 2014. His research interests include near-infrared neuronal modulation and auditory stimulation.

Wensheng Hou received his BS degree in physics from Southwest Normal University, Chongqing, China, in 1991. Then, he got his MS and PhD degrees in biomedical engineering from Chongqing

University, Chongqing, China, in 1998 and 2001, respectively. He spent one year as a visiting scholar for neural rehabilitation in the Psychology Department of the University of Surrey, UK. He is now a professor of biomedical engineering at the Chongqing University. His research interests focus on rehabilitation through neuromodulation, biomedical signal processing, and human–robot interaction.

Nan Xia is vice director of Shandong Provincial Key Laboratory of Digital Medicine and Computer-assisted Surgery at Qingdao University. In 2016, she received her doctoral degree in biomedical engineering from Chongqing University in China. She visited Northwestern University Feinberg School of Medicine Department of Otolaryngology as a joint PhD from 2013 to 2015. In 2017, she joined Qingdao University. Her research interest is auditory function restoration by using optical radiation.

Fei Peng received her doctorate degree in biomedical engineering from Chongqing University in China, in 2019. She is a postdoctoral fellow at the Department of Biomedical Science at the City University of Hong Kong. She worked at the University of Melbourne and Bionics Institute as a visiting PhD from 2016 to 2018. In 2019, she started to work at the City University of Hong Kong. Her research interest is to explore how the auditory system codes the statistical structure of natural sounds.

Xing Wang received her doctoral degree in biomedical engineering from Chongqing University in China in 2010. She is a lecturer at the Biomedical Engineering Department of Chongqing University. She visited John Hopkins University as a trainee PhD student from 2008 to 2009. Her research interest is auditory engineering and rehabilitation.

Xiaolin Zheng received his BS degree in electrical engineering from Chongqing University, Chongqing, China, in 1982. Then, he got his MS and PhD degrees in biomedical engineering from Chongqing University, Chongqing, China, in 1989 and 1995, respectively. He is now a professor of biomedical engineering at Chongqing University. His research interests include biomedical signal detection, neural stimulation, and bio-MEMS.

Xiaoying Wu received her BS degree in physics from Southwest Normal University, Chongqing, China, in 1991. She got her MS and PhD degrees in biomedical engineering from Chongqing University, Chongqing, China, in 2003 and 2010, respectively. She is now a professor in the Department of Biomedical Engineering at the Chongqing University. Her research interests include optical and electrical neural stimulation and rehabilitation engineering.

Biographies of the other authors are not available.